Prediction of Separation Angles Induced by Sharp Fins with Attack Angle

S. Koide*
Japan Defense Agency, Tokyo 190-8533, Japan

Introduction

GLANCING shock-wave/turbulent-boundary layer interaction, in which an oblique shock wave glances across a boundary layer along an adjacent wall (Fig. 1), constitutes one of the most important phenomena of three-dimensional interference. The primary separation line is one of the most easily discerned features of the interaction footprint obtainable by surface flow visualization. In the interaction induced by a sharp fin or a semicone, the separation line is usually straight except the "inception region." Hence once the angle of the separation line (β_s: defined as the angle formed by the separation line and the incoming freestream direction) is specified, one can grasp the extent of interaction region.

Koide et al.[1] previously proposed an empirical prediction method for the primary separation angles caused by a series of unswept sharp fins (USF) with attack angle α (Fig. 1a), semicones (SC), and sharp triangle fins (STF) at zero α (Figs. 1b and 1c). In the prediction, only the inviscid shock-wave characteristics such as shock angle and pressure rise across the shock were employed. (Inviscid means the imaginary condition that would exist if no boundary layer were presented on the wall.) In this Note, the prediction method is extended to include swept sharp fin (SSF) with α (Fig. 1d) and STF with α. Using the extended method, the separation angles can be predicted for almost all types of sharp shock generators with various angles of attack α, sweep angles λ, half-apex angles ε under a wide range of supersonic Mach numbers.

Methodology

As far as the inviscid flowfield is concerned, the wall is equivalent to the plane of symmetry for the delta wing as shown in Fig. 2. Hence the STF and SSF are treated as the half-cut model of the rhombic and flat delta wing, respectively. The inviscid-shock angle β_O, defined by the angle made by inviscid shock-wave trace on the wall with incoming freestream direction (Fig. 1), can be determined from the angle of shock trace on the symmetry plane.

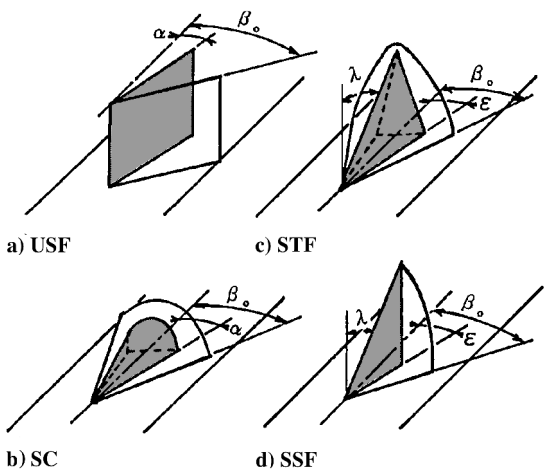

Fig. 1 Schematic views of several types of glancing interactions.

In the planar inviscid shock induced by USF, the pressure rise across the shock takes the form of a step. But in the case of conical shock, to which SC, SSF, and STF belong, the pressure behind the shock increases gradually toward the generator surface because of the conical nature of the flow. The overall pressure rise PR_{oa} (In the following, PR indicates a nondimensional pressure divided by the undisturbed incoming pressure.) is defined as the maximum pressure observed at the location of shock generator on the wall: at the ridge line in the case of the rhombic delta wing. On the other hand, the pressure rise just behind the shock PR_o is $(7M^2 \sin\beta_O - 1)/6$ for a specific heat ratio of 1.4 regardless of the type of inviscid shock.

Using β_O, PR_{oa}, and PR_o, the author confirmed that the relationship

$$\frac{\Delta\beta_s}{(PR_{oa}/PR_o)^4} = f(M_n) \tag{1}$$

could provide fairly accurate prediction of β_s for USF with α, STF, and SC at zero α (Ref. 1). In Eq. (1), $\Delta\beta_s$ is $\beta_s - \beta_O$, and Mn is the Mach number component normal to the shock wave ($\equiv M \sin\beta_O$). If independent variables of β_O and PR_{oa} in Eq. (1) can be specified for SSF and STF with α, β_s can also be predicted for such cases by the same way presented in Ref. 1.

Summary of Shock-Angle Prediction Method for STF with Angle of Attack

From Fig. 2, it is understood that β_O for STF at zero α (β_{OSTF}), SSF with α (β_{OSSF}), and STF with α ($\beta_{OSTF\alpha}$) correspond to β_O for

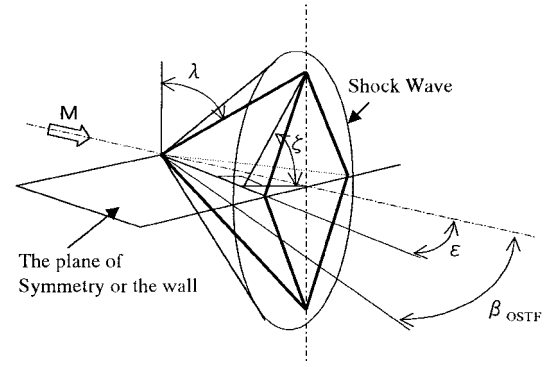

Rhombic delta wing with 0 alpha

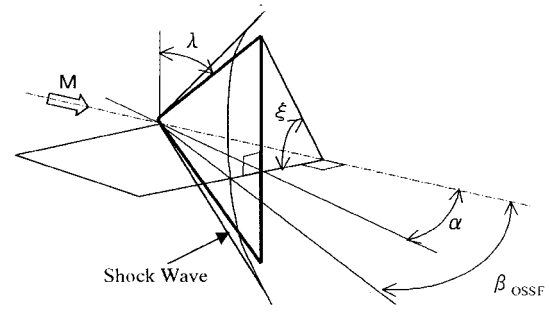

Flat delta wing

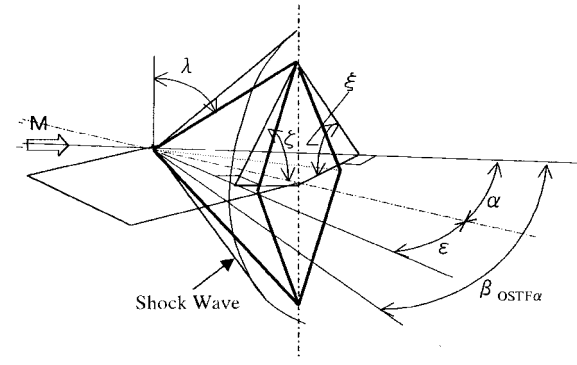

Rhombic delta wing with alpha

Fig. 2 Schematic views of rhombic and flat delta wing.

Received 5 May 2001; revision received 10 July 2001; accepted for publication 10 July 2001.

*Senior Research Engineer, Third Research Center, Technical R&D Institute, 1-2-10 Sakae, Tachikawa. Member AIAA.

the rhombic delta wing at zero α, flat delta wing with α, and the rhombic delta wing with α, respectively. Once the prediction method for β_{OSTF_α} is established, β_{OSTF} and β_{OSSF} can be treated as special cases of β_{OSTF_α}: β_{OSTF} is the value at zero α while β_{OSSF} at zero ε. In addition, β_{OSTF_α}, β_{OSTF}, and β_{OSSF} come close to $\beta_{OS}(\alpha+\varepsilon)$, $\beta_{OS}(\varepsilon)$, and $\beta_{OS}(\alpha)$, respectively, when λ approaches 0 deg [where $\beta_{OS}(x)$ is the theoretical two-dimensional oblique shock angle for a flow deflection angle of x]. Furthermore β_{OSTF} and β_{OSSF} become the Mach angle [$\mu = \sin^{-1}(1/M)$] when ε and α approach 0 deg. To establish the prediction method for β_{OSTF_α} while considering the preceding situations, the relationship

$$\beta_{OSTF_\alpha} = \frac{\beta_{OSTF}\beta_{OSFF}\beta_{OS}(\alpha+\varepsilon)}{\beta_{OS}(\alpha)\beta_{OS}(\varepsilon)} \tag{2}$$

was introduced in Ref. 2. Taking prediction procedures for β_{OSTF} and β_{OSSF} already presented in Ref. 2 into Eq. (2) yields

$$\beta_{OSTF_\alpha} = (\pi^2/4)(-0.13361 + 1.2459\zeta - 1.0576\zeta^2 + 0.3668\zeta^3) \times (-0.0202 + 1.0204\xi - 0.8885\xi^2 + 0.3234\xi^3) \times M^{(\pi-\xi-\zeta)/3}\beta_{OS}(\alpha+\varepsilon) \tag{3}$$

where ζ and ξ are

$$\zeta = \tan^{-1}(1/\sin\varepsilon \cdot \tan\lambda), \qquad \xi = \tan^{-1}(1/\sin\alpha \cdot \tan\lambda)$$

(Fig. 2). All angles in Eq. (3) are expressed in radians. Constants in the first parentheses of the right-hand side of Eq. (3) are different from those presented in Ref. 2 in order to simplify the equation with maintaining the accuracy of prediction.

Prediction of Shock Overall Pressure Rise for STF with Angle of Attack

For predicting the shock overall pressure rise for STF with attack angle PR_{oaSTF_α}, a similar procedure for β_{OSTF_α} has been employed. Like β_{OSTF_α} expressed by Eq. (2), PR_{oaSTF_α} is believed to be predicted as

$$PR_{oaSTF_\alpha} = \frac{PR_{oaSTF}PR_{oaSSF}PR_{OS}(\alpha+\varepsilon)}{PR_{OS}(\alpha)PR_{OS}(\varepsilon)} \tag{4}$$

where PR_{oaSTF} and PR_{oaSSF} are overall pressure rise for STF at zero α and SSF with α, respectively. $PR_{OS}(x)$ is the theoretical two-dimensional oblique shock pressure rise for a flow deflection angle of x.

To predict PR_{oaSTF_α} using Eq. (4), PR_{oaSTF} and PR_{oaSSF} have to be determined in advance. PR_{oa} cannot be found using a known simple method. However, the similar correlation procedure developed for predicting β_{OSTF} and β_{OSSF} also can be used to obtain PR_{oaSTF} and PR_{oaSSF}. Using computed values of PR_{oaSTF} for the rhombic delta wings with $8 \leqq \alpha \leqq 17$ deg, $30 \leqq \lambda \leqq 60$ deg, and $2.0 \leqq M \leqq 3.5$, the value of PR_{oaSTF} has been shown to be accurately predicted using the equation

$$PR_{oaSTF} = \left[\pi(0.0056\zeta + 0.398\zeta^2)PR_{os}(\varepsilon)\right]/2\zeta \tag{5}$$

The procedure of establishing the prediction method for PR_{oaSTF} is exactly the same as that of Ref. 2. But Eq. (5) is much simpler than the equation proposed in Ref. 2. This is mainly because the dependence of PR_{oa} on Mach number has been proved to be weaker than previously expected under Mach numbers examined. Hence a term including M has been erased, and then the correlation curve in the parentheses in Eq. (5) has been modified.

As to the prediction of PR_{oaSSF}, the same correlation procedure for PR_{oaSTF} has also been employed. A database of PR_{oaSSF} for the correlation was constructed using computational data by Klunker et al.[3] ($M = 4.0, 5.08$) and experimental data by Squire[4] ($M = 3.97$) for the flat delta wings. A similar relation,

$$PR_{oaSSF} = \left[\pi(0.4159\xi + 0.1367\xi^2)PR_{os}(\alpha)\right]/2\xi \tag{6}$$

has been proved to predict the value of PR_{oaSSF} accurately.

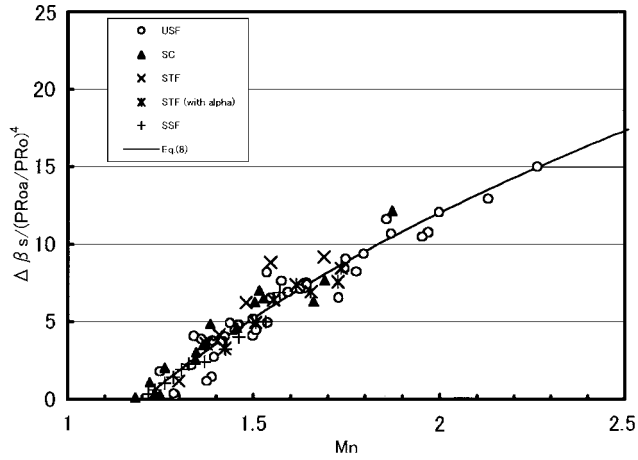

Fig. 3 Correlation of the separation angles in terms of shock angle and overall pressure rise.

Finally, PR_{oaSTF_α} can be expressed by substitution of Eqs. (5) and (6) into Eq. (4) as

$$PR_{oaSTF_\alpha} = (\pi^2/4)(0.0056 + 0.398\zeta)(0.4159 + 0.1367\xi)PR_{OS}(\alpha+\varepsilon) \tag{7}$$

Prediction of Separation Angles

Several data for β_s have been obtained experimentally by Lu et al.[5] ($M = 2.47$–3.95) and Rodi and Dolling[6] ($M = 4.9$) for USF; Settles and Lu[7] ($M = 2.95$) for SSF; Deng and Liao[8] ($M = 2.04, 2.5$), Avduyevskiy and Gretsov[9] ($M = 2.1, 2.9, 3.7$), and Saida et al.[10] ($M = 1.98, 2.49$) for SC; Saida et al.[11] ($M = 2.50$) for STF at zero α; and Matsuo[12] ($M = 2.5$) for STF with α. When they are plotted in M_n and $\Delta\beta_s/(PR_{oa}/PR_o)^4$ coordinates using Eqs. (3) and (7), most of the data points converge along a single line (Fig. 3). Why these coordinates can correlate the angles induced by dissimilar shock generators has already been explained in Ref. 1. Finally, the author has employed the relationship

$$\frac{\Delta\beta_s}{(PR_{oa}/PR_o)^4} = 23.654\,\ln M_n - 4.3503 \tag{8}$$

(depicted by the solid line in Fig. 3) to predict the separation angles β_s. In Ref. 1 a hyperbolic function of $7.8(Mn^2 - 1.3^2)^{1/2}$ was chosen as a correlation curve. But for all data presented in Fig. 3, the logarithmic expression in Eq. (8) has been confirmed to provide better prediction. The value of β_s predicted by Eq. (8) (expressed in degrees) has been shown to be fairy accurate [within 2 deg (1 deg) of the corresponding experimental value for 91% (68%) of the data points in Fig. 3]. As far as newly involved cases of STF and SSF with α are concerned, discrepancy between the predicted and experimental angle is trivial (at most 1.5 deg and 80% are within 1 deg).

Conclusions

A prediction method has been constructed for the primary separation angles of glancing shock-wave/turbulent boundary-layer interactions induced by dissimilar shock generators such as unswept sharp fin, swept sharp fin, swept triangle fin, and semicone. The separation angles are predicted by simple parameters comprising Mach number, the theoretical two-dimensional oblique-shock angle/pressure rise, and an angle representing the geometry of each swept sharp fin. Without time-consuming experiments and computational-fluid-dynamics calculations, this method can provide a rapid and reasonable estimation of the primary separation angle under supersonic Mach numbers.

References

[1] Koide, S., Saida, N., and Ogata, R., "Correlation of Separation Angles Induced by Glancing Interactions," *AIAA Journal*, Vol. 34, No. 10, 1996, pp. 2198–2200.

[2]Koide, S., Loria, A. F., and Babinsky, H., "Prediction of Shock Angles Caused by Sharp Delta Wings with Attack Angle," *AIAA Journal*, Vol. 36, No. 7, 1998, pp. 1327, 1328.

[3]Klunker, E. B., South, J. C., Jr., and Davis, R. M., "Calculation of Nonlinear Conical Flows by the Method of Lines," NASA TR R-374, Oct. 1971.

[4]Squire, L. C., "Pressure Distributions and Flow Patterns at $M = 4.0$ on some Delta Wings," British Aeronautical Research Council, Repts. and Memoranda, R&M 3373, London, Feb. 1964.

[5]Lu, F. K., Settles, G. S., and Horstman, C. C., "Mach Number Effects on Conical Surface Features of Swept Shock-Wave/Boundary-Layer Interactions," *AIAA Journal*, Vol. 28, No. 1, 1990, pp. 91–97.

[6]Rodi, P. E., and Dolling, D. S., "An Experimental/Computational Study of Sharp Fin Induced Shock Wave/Turbulent Boundary Layer Interactions at Mach 5: Experimental Results," AIAA Paper 92-0749, Jan. 1992.

[7]Settles, G. S., and Lu, F. K., "Conical Similarity of Shock/Boundary-Layer Interactions Generated by Swept and Unswept Fins," *AIAA Journal*, Vol. 23, No. 7, 1985, pp. 1021–1027.

[8]Deng, X. Y., and Liao, J. H., "Correlation of Conical Interactions Induced by Sharp Fins and Semicones," *AIAA Journal*, Vol. 31, No. 5, 1993, pp. 962, 963.

[9]Avduyevskiy, V. S., and Gretsov, V. K., "Investigation of a Three-Dimensional Separated Flow Around Semicones Placed on a Plane Plate," NASA TTF-13578, July 1971.

[10]Saida, N., Ooka, T., and Koide, S., "Interaction Between Shock Waves and Boundary Layer Induced by a Semicone Placed on a Flat Plate," *Journal of the Japan Society for Aeronautical and Space Sciences*, Vol. 33, No. 374, 1985, pp. 159–166 (in Japanese).

[11]Saida, N., Ogata, R., and Koide, S., "Shock Wave/Boundary Layer Interactions Induced by a Rhombic Delta Fin," *Journal of the Japan Society for Aeronautical and Space Sciences*, Vol. 48, No. 559, 2000, pp. 237–243 (in Japanese).

[12]Matsuo, K., "Shock Wave/Boundary Layer Interaction Induced by a Rhombic Delta Wing," M.S. Thesis, Dept. of Mechanical Engineering, Aoyama-Gakuin Univ., Setagaya, Tokyo, Jan. 2000 (in Japanese).

A. Plotkin
Associate Editor

Dynamics of an Orbiting Flexible Beam with a Moving Mass

D. C. D. Oguamanam* and J. S. Hansen†
University of Toronto, Toronto, Ontario M3H 5T6, Canada
and
G. R. Heppler‡
University of Waterloo, Waterloo, Ontario N2L 3G1, Canada

Introduction

THE operation of an early version of the International Space Station, in light of its large size and flexibility, gives reason to examine the effects that arise when the truss is traversed by the mobile servicing system. This has been partially investigated by Messac.[1,2]

Earth-based structures have been successfully modeled as elastic continua with traversing loads (or masses).[3–8] These studies highlight the influence of the magnitude of the traversing loads and the travel profile on the system dynamics. The dynamics of beams in general motion have been investigated by Ashley,[9] Sellappan and Bainum,[10] Kane et al.,[11] Meirovitch and Quinn,[12] Bainum and Li,[13] and Kirk and Lee.[14] The models in these studies can be looked upon as a satellite with an attached beam with a tip mass. The primary difference between these and the current study is that in the present work an additional mass is allowed to traverse the beam. The moving mass is modeled as a point mass, motion is restricted to the orbital plane, and the beam is modeled as an Euler–Bernoulli beam. Simulations are performed to examine the effect of various travel profiles on the system dynamics. Of particular interest are the elastic deformations under the moving mass and at the tip mass.

Mathematical Formulation

The system under consideration is shown in Fig. 1; motion is restricted to the orbital plane. A satellite, modeled as a massive rigid body with center of mass located at $S^\star$ and with distance a from the center of mass to the base of the beam, is in a circular orbit of radius R_c about the Earth's center O. Because the satellite body is assumed to be much more massive than the other parts of the system, the appendage attached to the satellite is modeled as a beam cantilevered in the satellite fixed frame. The beam carries a point mass payload m_t at the tip of the beam, and it is traversed by a point mass m_v. The orbital frequency is ω_o, and the satellite spin rate is $\dot{\theta}$ about an axis perpendicular to the plane of the orbit.

The dynamics of the system are described by the aid of an inertial frame located at O with the dextral orthogonal basis $\mathcal{F}_e^T = [\boldsymbol{e}_1, \boldsymbol{e}_2, \boldsymbol{e}_3]$; an orbital frame with dextral basis $\mathcal{F}^T = [\boldsymbol{o}_1, \boldsymbol{o}_2, \boldsymbol{o}_3]$ is also located at O and is oriented such that the $\boldsymbol{o}_1$ is always passing through $S^\star$; a satellite body-fixed frame with dextral basis $[\boldsymbol{s}_1, \boldsymbol{s}_2, \boldsymbol{s}_3]$ is attached at $S^\star$.

The position vectors from O, to a spacecraft differential mass element $\boldsymbol{R}_s$, to an elemental mass of the beam $\boldsymbol{R}_b$, to the moving mass $\boldsymbol{R}_v$, and to the tip mass $\boldsymbol{R}_t$ are

$$\boldsymbol{R}_i = \boldsymbol{R}_c + \boldsymbol{r}_i, \qquad i \in \{b, s, t, v\} \tag{1}$$

The kinetic energy of the system $\mathcal{T}$ is

$$\mathcal{T} = \frac{1}{2}\int_{m_s} \dot{\boldsymbol{R}}_s \cdot \dot{\boldsymbol{R}}_s \,\mathrm{d}m_s + \frac{1}{2}\int_{m_b} \dot{\boldsymbol{R}}_b \cdot \dot{\boldsymbol{R}}_b \,\mathrm{d}m_b + \frac{1}{2}m_v \dot{\boldsymbol{R}}_v \cdot \dot{\boldsymbol{R}}_v + \frac{1}{2}m_t \dot{\boldsymbol{R}}_t \cdot \dot{\boldsymbol{R}}_t \tag{2}$$

where the first and second terms are caused by the satellite and the appendage, respectively. The penultimate term is the contribution of the moving mass, and the last term is caused by the tip mass. The velocities may be expanded as

$$\dot{\boldsymbol{R}}_b = \mathcal{F}_s^T \begin{bmatrix} R_c\omega_o \sin\theta - (\dot{\theta} + \omega_o)w(x,t) \\ 0 \\ R_c\omega_o \cos\theta + (\dot{\theta} + \omega_o)(a + x) + \dot{w}(x,t) \end{bmatrix} \tag{3}$$

$$\dot{\boldsymbol{R}}_v = \mathcal{F}_s^T \begin{bmatrix} \dot{x}_v + R_c\omega_o \sin\theta - (\dot{\theta} + \omega_o)w(x,t) \\ 0 \\ R_c\omega_o \cos\theta + (\dot{\theta} + \omega_o)(a + x) + \dot{w}(x,t) + \dot{x}_v \left.\dfrac{\partial w}{\partial x}\right|_{x = x_v} \end{bmatrix} \tag{4}$$

$$\dot{\boldsymbol{R}}_t = \dot{\boldsymbol{R}}_b(L_b, t) \tag{5}$$

where the angular velocity of the satellite with respect to the inertial frame is

$${}^E\boldsymbol{\omega}^s = -(\dot{\theta} + \omega_o)\boldsymbol{e}_2 \tag{6}$$

The time derivative of the deformation under the moving mass position $\mathrm{d}w/\mathrm{d}t$ introduces a convective term, which is a product of the moving mass speed and the slope of the deformation at the location of interest, as observed in Eq. (4).

The total potential energy is composed of the gravitational potential $\mathcal{U}_G$ and the strain energy $\mathcal{U}_S$:

$$\mathcal{U}_G = -\mu\left\{\int_{m_s} |\boldsymbol{R}_s|^{-1}\,\mathrm{d}m_s + \int_{m_b} |\boldsymbol{R}_s|^{-1}\,\mathrm{d}m_b + m_v|\boldsymbol{R}_v|^{-1} + m_t|\boldsymbol{R}_t|^{-1}\right\} \tag{7}$$

$$\mathcal{U}_S = \frac{1}{2}\int_0^{L_b} EI\left(\frac{\partial^2 w}{\partial x^2}\right)^2 \mathrm{d}x \tag{8}$$

Received 29 December 2000; revision received 10 July 2001; accepted for publication 10 July 2001.

*Postdoctoral Fellow, Institute for Aerospace Studies, 4925 Dufferin Street.
†Professor, Institute for Aerospace Studies, 4925 Dufferin Street.
‡Professor, Systems Design Engineering. Senior Member AIAA.